JOURNAL OF SOLID STATE CHEMISTRY 43, 299–308 (1982)

Structural Relationships in the Series $A_xP_4O_8(WO_3)_{2m}$ (A = K, Rb): A High-Resolution Electron Microscopy Study

M. HERVIEU AND B. RAVEAU

Laboratoire de Cristallographie et Chimie du Solide, L.A. 251, ISMRA-Université de Caen, 14032 Caen Cedex, France

Received February 3, 1982; in final form March 31, 1982

The first members of the series $A_xP_4O_8(WO_3)_{2m}$ were studied by means of electron microscopy. These bronzes can be classified into two groups on the basis of ReO_3-type block composition: even- and odd-m members. High-resolution lattice images of tungstophosphate crystals ($m \leq 10$) allow us to establish a correlation between the image contrast and the framework of the structure. The structural mechanism proposed for this series is discussed and compared to the possibility of intergrowth, and to the crystallographic shear phenomena observed in tungsten and molybden oxides.

Introduction

Previous X-ray diffraction studies of two compounds $Rb_xP_8W_{24}O_{88}$ (*1*) and $Rb_xP_8W_{32}O_{112}$ (*2*) let us foresee the possibility of the existence of a large family of microphases corresponding to the general formula $A_xP_8W_{8n}W_{24n+16}$, n being an integer. The close structural relations between these members led us to investigate compositions corresponding to nonintegral n values which would involve intergrowths of two such structures, as recently observed for several tunnel oxides (*3–8*). However, the arrangement of the polyhedra let us consider for $n = i + \frac{1}{2}$ another structural hypothesis which would be related to the crystallographic shear phases (*9–13*) involving the general formula $A_xP_4O_8(WO_3)_{2m}$, m always being an integer ($m = 2n$).

On the other hand, no investigation of such compounds including potassium has been made for this structural type. Thus, the present work deals with the electron microscopy study of the first members of the series $A_xP_4O_8(WO_3)_{2m}$, with A = K and Rb.

Previous Structural Results and Cell Parameters of the Even-m Members

The projection on to the (010) plane of the idealized structure of the member $m = 6$, $Rb_xP_4W_{12}O_{44}$, is shown as an example in Fig. 1. The host lattice of these compounds can be described as built up from ReO_3-type slabs, connected through P_2O_7 groups. From this figure, it can be seen that all the even-m members of the family $A_xP_4O_8(WO_3)_{2m}$ should exhibit a monoclinic cell, with parameters closely related to the "a_{ReO_3}" parameter. Along $[001]_{ReO_3}$ direction of the ReO_3-type subcell, this framework can indeed be considered as built up from strings of $m/2$ corner-sharing WO_6 octahedra (here $m/2 = 3$) limited at both ends by one PO_4 tetrahedron, while in the normal direction $[110]_{ReO_3}$, the periodicity of the

0022-4596/82/090299-10$02.00/0

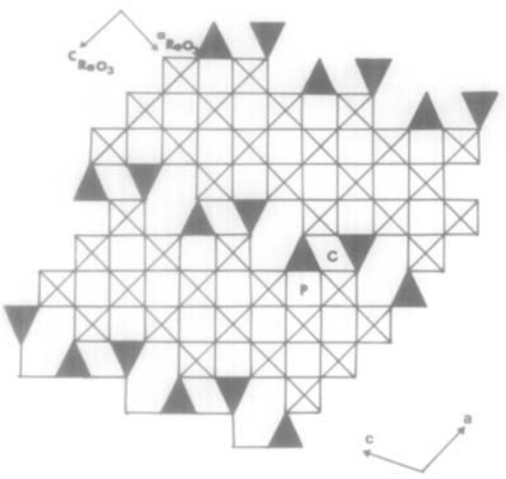

FIG. 1. Idealized drawing of the monoclinic structure of $AP_4W_{12}O_{44}$ ($m = 6$) projected onto the (010) plane. The black triangles represent P_2O_7 groups.

perovskite slab is obtained for strings of m corner-sharing octahedra limited in the same way by one PO_4 tetrahedron at each end. If we choose the "a" parameter of the monoclinic cell of these oxides as a characteristic of width of the ReO_3-type slabs, i.e., parallel to $[001]_{ReO_3}$, its ideal value will be given by the relation

$$a \simeq \tfrac{1}{2}m\, a_{ReO_3} + K. \qquad (1)$$

The constant K characterizes the thickness of the rows of distorted hexagonal tunnels (or planes of PO_4 tetrahedra) which separate two successive ReO_3-type slabs, and corresponds approximatively to the edge of a tetrahedron and is thus close to $a_{ReO_3}/2^{1/2}$.

The a and b directions, as well as the β angle, will be the same for all the even-m members of the series, if we do not take on account slight variations due to the apparent change of oxidation state of W, which can also influence the distortion of the framework. The b parameter which corresponds to the $[010]_{ReO_3}$ direction will be twice that of the ideal perovskite, owing to the presence of the P_2O_7 groups (Fig. 2), which can be considered as replacing two octahedra in the ReO_3-type structure. The c parameter is parallel to the rows of distorted hexagonal tunnels and will only depend on the a_{ReO_3} parameter. Thus the relationships between these parameters and those of ReO_3 are given by the following relations:

$$b \simeq 2a_{ReO_3}, \qquad (2)$$

$$c \simeq a_{ReO_3}\, 20^{1/2}, \qquad (3)$$

$$\cos\beta \simeq -5^{1/2}/5, \qquad \beta \simeq 116°57. \qquad (4)$$

This framework is favorable for an electron microscopy study since it forms tunnels parallel to b and thus zones of weak electron density which can be distinguished from the zones of high electron density where the files of octahedra and tetrahedra are located. Three sorts of tunnels are indeed observed. Moreover, two of them are empty: the perovskite tunnels P located in the ReO_3-type slabs, and the C tunnels formed by two tetrahedra and two octahedra and located at the boundary of the ReO_3-type slabs. The distorted hexagonal tunnels located at the boundary of two slabs are very large and have only half of their sites occupied by the A ions.

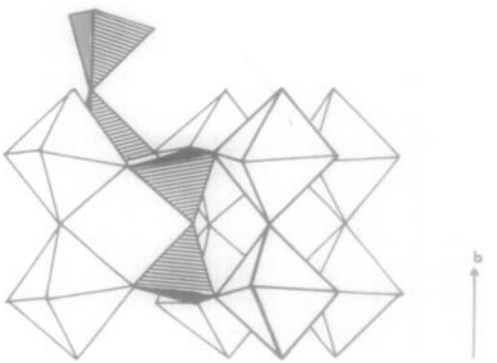

FIG. 2. Connection of octahedra and P_2O_7 groups: one P_2O_7 group can be considered as replacing two octahedra in the ReO_3 structure.

Experimental

Synthesis. For this study, the problem of nonstoichiometry due to insertion has not been investigated, owing to the previous observations of the rubidium bronzes which have shown that the composition range of these phases is rather narrow (*1*, *2*). Thus only the bronzes corresponding to the compositions $AP_4O_8(WO_3)_{2m}$, with m integer, $m \leq 10$, and A = K and Rb, have been investigated. Mixtures of $H(NH_4)_2PO_4$, A_2CO_3, and WO_3 were heated in air at 873 K in platinum crucibles in order to decompose the ammonium phosphate and the alkali carbonates. Then, metallic tungsten was added and mixed with the resulting compounds in order to obtain the stoichiometric composition. In a second step the mixtures were heated in a silica ampoule and sealed under vacuum at 1373 K during 15 days. The color of the bronzes varies gradually from dark blue to black.

X-Ray diffraction analysis. The samples were first identified with a Guinier de Wolff camera. The X-ray diffractograms were then registered on a Philips goniometer using the Cu$K\alpha$ radiation in order to determine the cell parameters with accuracy.

Electron microscopy study. The samples for the electron diffraction microscopy study were ground in alcohol and laid on a carbon grid. They were studied with a Jeol microscope 100 CX, using in a first step a goniometric stage (±60°C) for electron diffraction, then in a second step a high-resolution stage.

Results and Discussion

The first member of the series which would involve P_4O_{10} groups has not been observed. The phases corresponding to m = 2 and m = 3 could not be synthesized: mixtures of $P_8W_{12}O_{52}$ (*14*) and $K_2P_8W_{16}O_{64}$ (*15*), whose structure is related to those of Mo_4O_{11} (*16*, *17*), were identified. Seven phases of $AP_4O_8(WO_3)_{2m}$ were synthesized for A = Rb (m = 4 to 10) and six for A = K (m = 5 to 10).

X-Ray Study and Electron Diffraction Study

All the compositions were studied by electron diffraction and X-ray diffraction in order to determine their space group and also to test their homogeneity.

No superstructure line or reflection corresponding to a doubling of the b parameter with respect to that of ReO_3 has been observed by X-ray diffraction, whatever the composition of the sample may be. Moreover, the electron diffraction observations have always shown a doubling of the b parameter ($b = 2a_{ReO_3}$) as shown from Fig. 3a, where the ($0kl$) plane of the member m = 6 is presented, with the limiting reflection

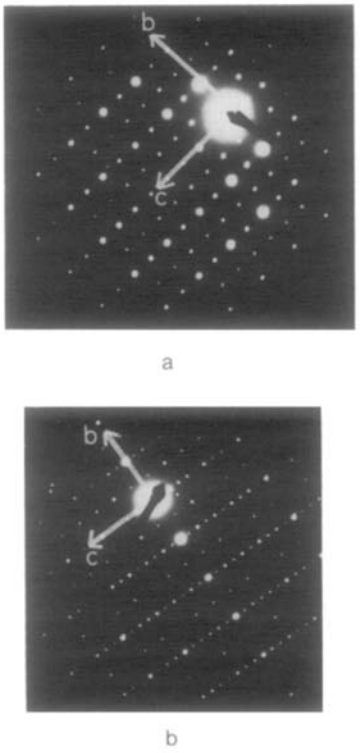

FIG. 3. Electron diffraction patterns of ($0kl$) planes: (a) m = 6; (b) m = 8.

TABLE I

$AP_4O_8(WO_3)_{2m}$: CRYSTALLOGRAPHIC DATA

m	Composition	Ref.	a (Å)	b (Å)	c (Å)	β
4	$RbP_4W_8O_{32}$	[a]	10.19_6	$2 \times 3.76_2$	17.15_4	113°32
6	$KP_4W_{12}O_{44}$	(*18*)	14.00_6	$2 \times 3.76_5$	17.05_6	114°30
	$RbP_4W_{12}O_{44}$	(*18*)	13.99_4	$2 \times 3.74_9$	17.12_8	114°30
8	$KP_4W_{16}O_{56}$	(*19*)	18.19_5	$2 \times 3.77_0$	17.08_7	117°30
	$RbP_4W_{16}O_{56}$	(*19*)	18.21_3	$2 \times 3.77_4$	17.09_5	117°39
10	$KP_4W_{20}O_{68}$	[a]	21.38_6	$2 \times 3.76_7$	16.96_8	113°57
	$RbP_4W_{20}O_{68}$	[a]	21.39_5	$2 \times 3.77_6$	17.063	113°93
5	$KP_4W_{10}O_{38}$	[a]	11.06_1	$2 \times 3.75_0$	17.13_3	93°78
	$RbP_4W_{10}O_{38}$	[a]	11.09_1	$2 \times 3.76_1$	17.14_0	93°78
7	$KP_4W_{14}O_{50}$	[a]	14.61_8	$2 \times 3.75_4$	17.09_8	98°99
	$RbP_4W_{14}O_{50}$	[a]	14.63_8	$2 \times 3.76_7$	17.07_0	99°00
9	$KP_4W_{18}O_{62}$	[a]	18.14_3	$2 \times 3.76_6$	17.12_0	101°54
	$RbP_4W_{18}O_{62}$	[a]	18.06_9	$2 \times 3.77_8$	17.16_3	102°53

[a] This work.

conditions $k + l = 2n$ (space group $A2/m$), and from Fig. 3b, where the $(0kl)$ plane of the member $m = 8$ is presented with the reflection conditions $0k0$, $k = 2n$ (space group $P2_1/c$). This is in agreement with the X-ray diffraction results observed for the rubidium bronzes corresponding to $m = 6$ and $m = 8$. The previous X-ray study of the oxides on single crystals (*1*, *2*) did not exhibit any superstructure reflections involving a b parameter twice that of ReO_3; however, the final resolution of the structures showed a splitting of some oxygen atoms and an occupancy factor of the phosphorous sites which imposed a doubling of the b parameter; this has been confirmed by the electron diffraction study of these phases.

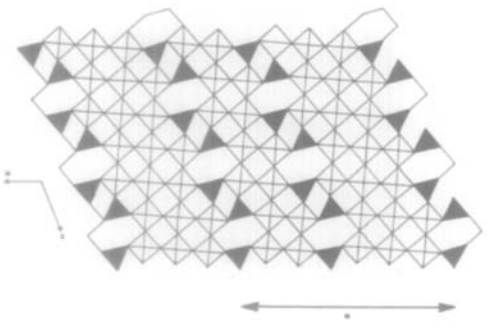

FIG. 4. Idealized drawing of a hypothetical structure for the intergrowth of $m = 4$ and $m = 6$.

Accurate lattice parameters were obtained after the X-ray powder patterns were indexed. As shown from Table I, all the oxides are monoclinic and are characterized by very close b and c parameters ($b \simeq 2a_{ReO_3}$; $c \sim a_{ReO_3}20^{1/2}$) whatever the m values may be, even or odd. The observed parameters of the monoclinic cell of the even-m members do agree with those previously predicted. The b and c parameters of the odd-m members show clearly that these compositions are also built up from ReO_3-type slabs; the a parameter values do not agree with an intergrowth of two even-m members along this direction (Fig. 4). This is confirmed by the β value, which is different from that of the even members, and corresponds to a shift of two successive rows of distorted hexagonal tunnels as will be

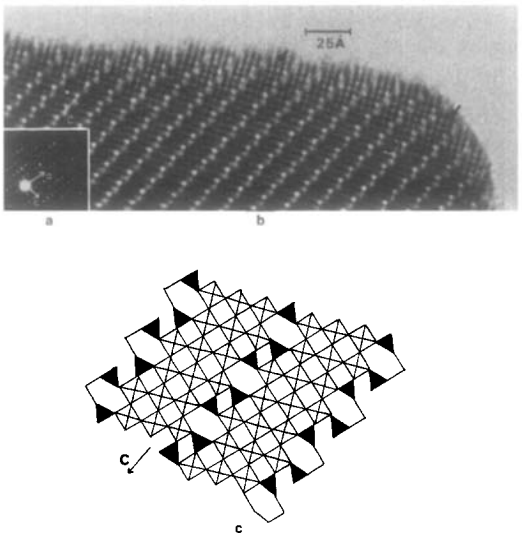

FIG. 5. $KP_4W_{12}O_{44}$. (a) Electron diffraction pattern of $(h0l)$. (b) High-resolution micrograph of $m = 6$. (c) Crystal structure projected onto the (010) plane. Black arrows = defects, such as $m = 7$ members.

shown without ambiguity from the high-resolution study of these members.

It must be pointed out that besides the microcrystals described here, the electron diffraction observations show that a minority of crystals—about 10 to 20%—exhibit electron diffraction patterns somewhat different in the $(h0l)$ plane. One observes superstructure reflections corresponding to an absence of extinction along c, which are more or less intense. A systematic study of this phenomenon is in progress.

Electron Microscopy Resolution

The high-resolution lattice images obtained for this structural family are given in Figs. 5, 6, 7, 8, and 9.

Diaphragms with 40- and 60-μm diameters were used in order to limit the number of diffracted beams and to increase the contrast. For this study, we selected microcrystals whose b axis was parallel to the electron beam. So, for example, for $m = 6$, about 140 beams contribute to the formation of the image presented here.

The nature of the observed image contrast depends on the objective lens defocus and on the thickness of the crystal. All the micrographs exhibit bands of white dots, separated by zig-zag ribbons, which are white or black and parallel to the c direction. Every member was identified by the superstructure spots in its diffraction pattern and the dimensions of the repeating unit of the image contrast. Their interpretation for a great number of microcrystals allowed us to test the homogeneity of the preparation with respect to the nominal composition and to test the regularity of the distribution of the ReO_3-type slabs within the same microcrystal. Although we must be careful with the interpretation of the high-resolution images in terms of polyhedra or tunnels, it will be seen that the correlation of the images of some even-m members whose structure is known with the arrangement of their tunnels is very strong. This allows us to generalize this interpretation to the other members of the series.

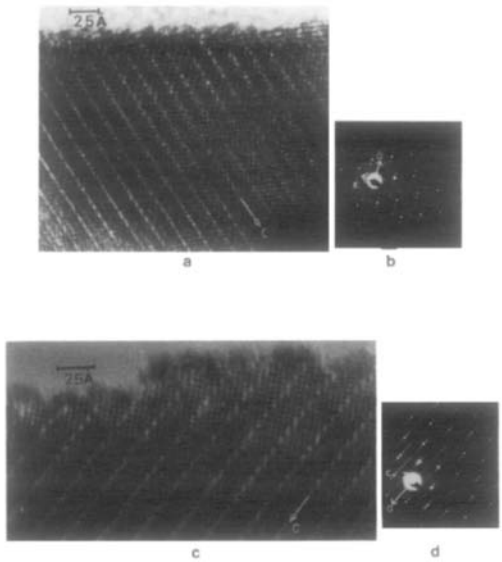

FIG. 6. (a) High-Resolution micrograph of $m = 8$ member, $KP_4W_{16}O_{56}$, viewed along b. (b) Its electron diffraction pattern. (c) High-resolution micrograph of $m = 10$, $KP_4W_{20}O_{68}$. (d) Its electron diffraction pattern.

Even-m Members Lattice Images

Micrograph 5b presents an image recorded for an $m = 6$ crystal; white spots slabs, about 14 Å wide, are separated by white ribbons in which an intense white spot alternates with a weaker one located at about 8.5 Å. As a result, the two and three white spots along the $[001]_{ReO_3}$ direction separated by strong white maxima will correspond, respectively, to two and three perovskite tunnels and to a distorted hexagonal tunnel: in the same way, the five white spots observed in a normal direction which alternate with a strong white maximum will also correspond to five perovskite tunnels and one hexagonal tunnel, respectively. The geometric relations between these white spots are in agreement with the projection of the structure onto the (010) plane (Fig. 5c).

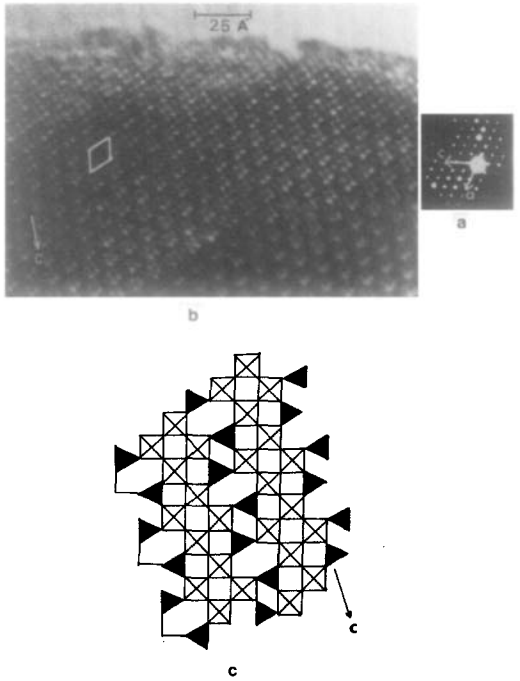

FIG. 7. $RbP_4W_8O_{32}$. (a) Electron diffraction pattern of $(h0l)$. (b) High-resolution micrograph of $m = 4$ member viewed along b. (c) Crystal structure of $RbP_4W_8O_{32}$ projected onto the (010) plane.

Two other even-m members, $m = 8$ and $m = 10$, of the $KP_4O_8(WO_3)_{2m}$ family are shown on Fig. 6. m values were determined, as previously described, by electron diffraction patterns and by length measures of repeating units of contrasts; examination of these images using the previous correlations enabled us to check the homogeneity of every crystal.

The images recorded for an $m = 4$ rubidium bronze crystal (Fig. 7b) show inverse shape and contrast; again, the image contrast consists of white spot arrays, parallel to the c axis, in a darker background but the slabs are separated by dark ribbons. In these ribbons two weak white dots (sometimes darkened) alternate with a strong dark maximum. The repeating unit of contrast is outlined by white strokes on Fig. 7b; its dimensions are those of the monoclinic cell determined from the X-ray diffractogram. A satisfactory interpretation of the contrast, geometric relations, and the numbers of spots in the bands (in $[100]_{ReO_3}$ and $[001]_{ReO_3}$ directions) is obtained if a correlation between white maxima and the heavy electronic density is assumed. Figure 7c allows us to check this contrast correlation with the projection of the idealized structure of the member $m = 4$.

Odd-m Members Resolution

During this study, single crystals of the member $m = 7$, $KP_4W_{14}O_{50}$, were isolated; their structure was studied and is going to be published (*20*). This work and the electron diffraction results clearly show that the members corresponding to odd-m values could not be considered as intergrowths of two even-m members in which ReO_3-type slabs, with different widths, would alternate.

The micrograph of the member $m = 5$ (Fig. 8b), which has been identified by its electron diffraction pattern (Fig. 8a), can be interpreted by comparison with that of the

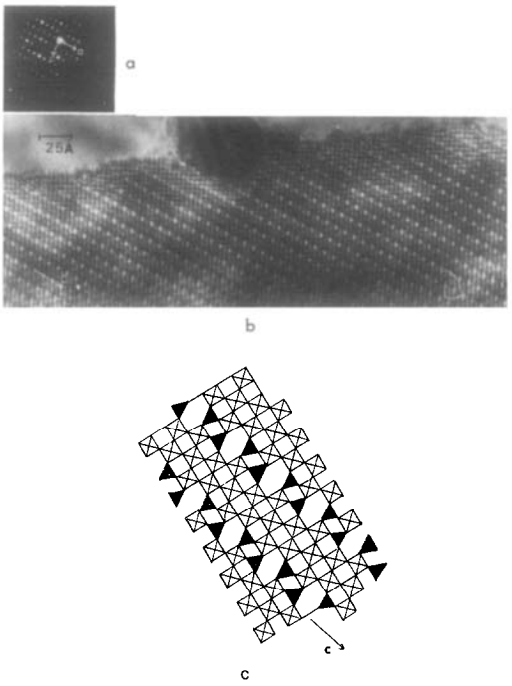

FIG. 8. $KP_4W_{10}O_{38}$. (a) Electron diffraction pattern of $(h0l)$. (b) High-resolution micrograph. (c) Crystal structure projected onto (010) plane of $m = 5$ member.

even member $m = 6$, assuming that the white spots can be attributed to zones of weak electron density, i.e., to tunnels. White ribbons formed of intense white spots alternating with weaker white spots can be identified as corresponding to rows of distorted hexagonal tunnels built up from P_2O_7 groups and WO_6 octahedra: in these ribbons, the more intense spots correspond to the hexagonal tunnels, while the weaker ones correspond to the tunnels characterized by a rhombic section. Between two such files, white spots, arranged as in a checkerboard are observed; these white spots can be attributed to the perovskite tunnels belonging to the ReO_3-type slabs. The distribution of these spots with respect to those of the ribbons allows us to propose the structural model of Fig. 8c: along the $[100]_{ReO_3}$ direction, four white spots (perovskite tunnels) in a periodic manner, while in the normal direction, two white spots (perovskite tunnels) are alternately separated by an intense white spot (hexagonal tunnels) and a weak white spot (rhombic tunnel).

The framework of all the odd-m members of the series can now be predicted. It is built up from rows of distorted hexagonal tunnels formed of corner-sharing octahedra and P_2O_7 groups identical to those observed for the even-m members. The main differences between these two series concern the relative positions of two successive rows which are shifted along the c direction. The result is that the ReO_3-type slabs between two rows will not have a constant width but will be formed of strings of octahedra which are transverse with respect to the tunnel rows and alternately built up from $(m - 1)/2$ and $(m + 1)/2$ octahedra. The principle of formation of such a lattice can be better understood by examination of Fig. 8c for $m = 5$: each ReO_3-type slab consists of strings which are alternately two octahedra and three octahedra long and are limited by two P_2O_7 groups: along the $[001]_{ReO_3}$ direction a string of two octahedra is connected to a string of three octahedra through a P_2O_7 group.

From these observations, the parameters of the monoclinic cell, and especially their relations with the ReO_3 cubic cell, can be given. Along two directions, which are parallel to the ReO_3-type layers, the parameters will be the same as those of the integral members, while the third parameter, a, corresponding to the width of the ReO_3-type layer will be different:

$$a = a_{ReO_3} \times [|(m - 1)/2|^2 + 1]^{1/2} + K \quad \text{with } K \sim a_p/2^{1/2},$$

$$b \simeq 2a_{ReO_3},$$

$$c \simeq a_{ReO_3}\, 20^{1/2},$$

$$\beta \sim 116°57 - \omega \quad \text{with tg } \omega = 2/(m - 1).$$

These calculated parameters agree with those observed from the X-ray and electron diffraction patterns.

The high-resolution images of the members $m = 7$ and $m = 9$ confirm this structural model. For $m = 7$ (Fig. 9), an inverse contrast is observed with respect to $m = 5$. In the micrograph of this member (Fig. 9a), which consists of bands of white spots distributed as in a checkerboard, and separated by dark ribbons, the white spots can easily be identified to the octahedra of the ReO_3-type slabs, while the dark spots of the ribbons correspond to the hexagonal tunnels (Fig. 9b) in agreement with the structural study of this phase (*20*). In the same way, the micrograph of the term $m = 9$ (Fig. 10a) shows that its structure (Fig. 10b) is built up from ReO_3-type slabs in which strings of four octahedra alternate with strings of five octahedra.

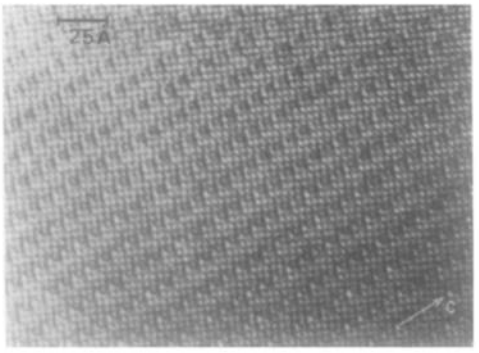

a

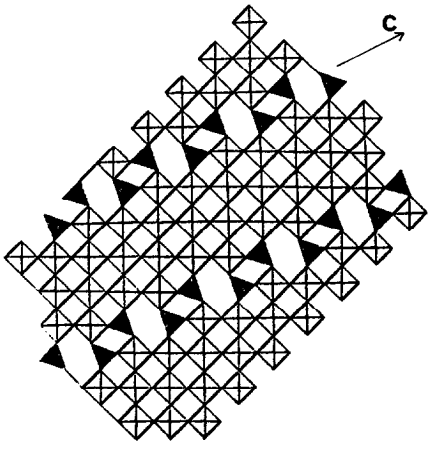

b

FIG. 9. $KP_4W_{14}O_{50}$. (a) Lattice image of $m = 7$ member. (b) Idealized drawing of the monoclinic structure projected onto the (010) plane.

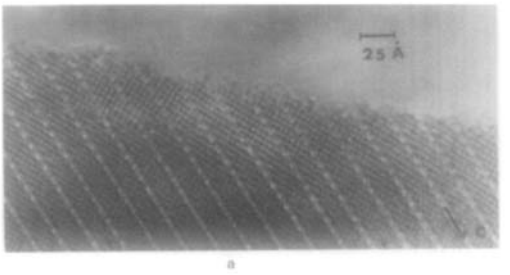

a

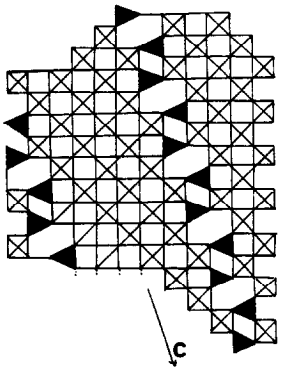

b

FIG. 10. $KP_4W_{18}O_{62}$. (a) Lattice image of $m = 9$ member. (b) Idealized drawing of the structure projected onto the (010) plane. (Black arrows = defects, such as $m = 8$ and 10 members.)

Possibility of Formation of Defects

Whatever the m value may be, even or odd, it is worthy of note that the majority of the crystals which were investigated were of good quality and generally exhibit a great regularity in the distribution of the ReO_3-type slabs. It must, however, be pointed out that this regularity tends to decrease when m increases. So, for the nominal composition $RbP_4W_8O_{32}$ ($m = 4$), the crystals do not exhibit any defects which would correspond to the local presence of members

with $m \neq 4$. However, for the nominal composition $KP_4W_{20}O_{68}$ ($m = 10$) many crystals exhibit, besides wide regular regions corresponding to the members $m = 10$, some perturbations due to the presence of members with $m \neq 10$; for this composition, only some crystals are very irregular: their electron diffraction patterns exhibit diffusion streaks parallel to a, and strongly perturbed zones corresponding to the presence of members with $m = 8$, 9, and 14 are observed (Fig. 11).

Conclusion

This electron microscopy study confirms the structural mechanism which was recently proposed for all the even-m members of the series $AP_4O_8(WO_3)_{2m}$ (*1*, *2*). On the other hand, the investigation of the odd-m members shows that they must be considered as new members which do not result from the intergrowth of even members but correspond to the shifting of two successive rows of tunnels with respect of one to the other. However, considering the number of octahedra which determine the width of the ReO_3-type slabs along $[100]_{ReO_3}$ direction instead of the $[001]_{ReO_3}$ let appear a continuous series, whatever the m value may be, odd or even. Then, assuming the tetrahedral planes to be parallel to $(102)_{ReO_3}$, a close similarity between these phases and those of {102} crystallographic shear phases (*9*) must be pointed out. It appears that these microphases are very stable since most of the crystals are regular. Members corresponding to high m values ($m > 10$) and nonintegral values will be investigated in order to determine the possibilities of defect and of nonstoichiometry in these compounds.

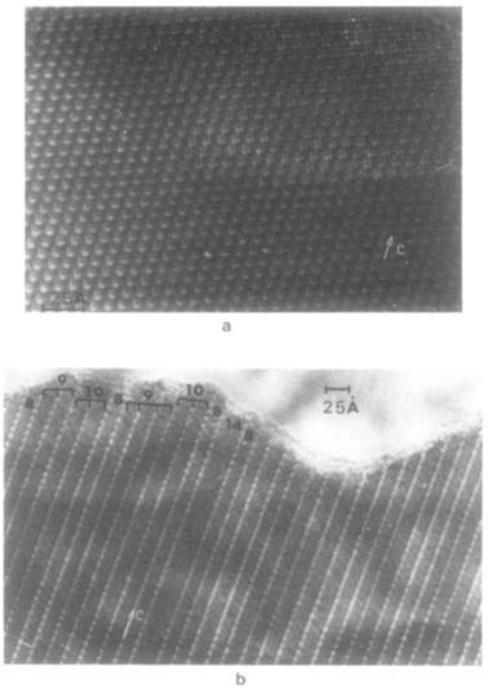

FIG. 11. Lattice images of (a) a well-ordered crystal of $m = 4$ member, and (b) a disordered crystal ($m = 10$) exhibiting different members: $m = 8$, 9, and 14.

References

1. J. P. GIROULT, M. GOREAUD, PH. LABBÉ, AND B. RAVEAU, *Acta Crystallogr. Sect. B* **37,** 1163 (1981).
2. J. P. GIROULT, M. GOREAUD, PH. LABBÉ, AND B. RAVEAU, *Acta Crystallogr. Sect. B* **36,** 2570 (1980).
3. A. HUSSAIN AND L. KIHLBORG, *Acta Crystallogr. Sect. A* **32,** 551 (1976).
3. S. IJIMA AND J. G. ALLPRESS, *Acta Crystallogr.* **130,** 29 (1974).
5. M. PARMENTIER, C. GLEITZER, AND R. J. D. TILLEY, *J. Solid State Chem.* **31,** 305 (1980).
6. F. STUDER AND B. RAVEAU, *Phys. Status Solidi A* **48,** 301 (1978).
7. F. STUDER AND B. RAVEAU, *Phys. Status Solidi A* **49,** 189 (1978).
8. M. HERVIEU, F. STUDER, AND B. RAVEAU, *Phys. Status Solidi A* **60,** 237 (1980).
9. A. MAGNELI, *Acta Crystallogr.* **6,** 495 (1953).
10. A. D. WADSLEY, *Rev. Pure Appl. Chem.* **5,** 165 (1965).
11. A. MAGNELI, B. BLOMBERG-HANSSON, L. KIHLBORG, AND G. SUNDKVIST, *Acta Chem. Scand.* **9,** 1382 (1955).
12. R. J. D. TILLEY, *Mater. Res. Bull.* **5,** 813 (1970).
13. J. G. ALLPRESS, R. J. D. TILLEY, AND M. J. SIENKO, *J. Solid State Chem.* **3,** 440 (1971).

14. B. DOMENGES, M. GOREAUD, PH. LABBÉ, AND B. RAVEAU, *Acta Crystallogr.*, in press.
15. J. P. GIROULT, M. GOREAUD, PH. LABBÉ, AND B. RAVEAU, *J. of Solid State Chem.* **44,** (1982).
16. A. MAGNELI, *Acta Chem. Scand.* **2,** 861 (1948).
17. L. KIHLBORG, *Acta Chem. Scand.* **13,** 954 (1959).
18. J. P. GIROULT, M. GOREAUD, PH. LABBÉ, J. PROVOST, AND B. RAVEAU, *Mater. Res. Bull.* **16,** 811 (1981).
19. J. P. GIROULT, Thèse de Docteur Ingénieur, University of Caen, Sept. 1981.
20. J. P. GIROULT, M. GOREAUD, PH. LABBÉ, AND B. RAVEAU, *Acta Crystallogr.*, in press.